

# Modeling and Analysis of Vibration Characteristics of Complex Boundary Annular Plate Under Thermal Environment

ZHU Ziyuan, XU Ruikang, WANG Gang\*

School of Mechanical and Electric Engineering, Soochow University, Suzhou 215131, P. R. China

(Received 3 February 2023; revised 17 March 2023; accepted 5 April 2023)

**Abstract:** Annular plate structure is widely used in the engineering field. A unified method is proposed to predict the free vibration behavior of the annular plates in the steady-state thermal environment. Based on the spectral geometry method (SGM), the displacement of the annular plate is expanded by the improved Fourier series. The potential energy and the maximum kinetic energy of the annular plate are obtained based on the first-order shear deformation theory (FSDT). Three sets of linear springs and one set of rotating springs are used to simulate the arbitrary boundary of the annular plate. The continuity of the circumferential boundary of the annular plate with subtended angle of  $360^\circ$  is realized by using circumferential coupling spring. The Rayleigh-Ritz method is used to construct the theoretical model of the annular plate, and the vibration characteristics of the annular plate are solved. The accuracy of this method is verified by comparing with the finite element calculation results. The method used in this paper is a meshless method, which is more computationally efficient than current mainstream methods, such as the finite element method (FEM). The relationships between the modal numerical solution and boundary condition and the ratio of inner and outer radius in the thermal environment are studied. This paper provides a reference for the application of annular plates in engineering practice.

**Key words:** annular plate; spectro-geometric method; thermal environment; Rayleigh-Ritz method

**CLC number:** TB31      **Document code:** A      **Article ID:** 1005-1120(2023)03-0273-12

## 0 Introduction

Plate structures have a wide range of applications in the fields of marine engineering, aerospace engineering, and mechanical engineering, making it essential to study and control their vibration<sup>[1]</sup>. The annular plate is a typical type of rotary plate. Compared with common fan and round plates, annular plates have many advantages, such as maintaining a certain degree of stiffness with reduced mass and having a certain degree of heat and sound absorption. As annular plates are a type of thin plate structure, they are highly sensitive to temperature and it is necessary to analyze the vibration characteristics of annular plates in the thermal environment.

Irie et al.<sup>[2]</sup> used the transfer matrix method to derive dimensionless frequency parameters for the

free vibration of annular plates. Due to its good convergence, the discrete singular convolution (DSC) method<sup>[3-6]</sup> has also been fully applied in the plate and shell modeling. In addition, the semi-analytic polynomial method (SAPM)<sup>[7-8]</sup> and the generalized differential quadrature method (GDQM)<sup>[9-10]</sup> have also been studied by many scholars and applied in several fields, such as free vibration and nonlinear dynamic analysis of plate and shell structures. Han et al.<sup>[11]</sup> performed a numerical analysis of the axisymmetric free vibration of a medium-thick plate using the differential product method (DQM). Tornabene et al.<sup>[12]</sup> studied the dynamics of medium-thickness functional gradient annular plates based on first-order shear deformation theory (FSDT) and the two-dimensional differential product method.

\*Corresponding author, E-mail address: wanggang81@suda.edu.cn.

**How to cite this article:** ZHU Ziyuan, XU Ruikang, WANG Gang. Modeling and analysis of vibration characteristics of complex boundary annular plate under thermal environment[J]. Transactions of Nanjing University of Aeronautics and Astronautics, 2023, 40(3): 273-284.

<http://dx.doi.org/10.16356/j.1005-1120.2023.03.004>

Efraim et al.<sup>[13]</sup> used FSDT to investigate the free vibration characteristics of isotropic annular plates of variable thickness. Ke et al.<sup>[14]</sup> studied the bending, buckling, and free vibration of annular plates of functional gradient materials based on the modified coupled stress theory and the Mindlin plate theory. Gürses et al.<sup>[15]</sup> analyzed the free vibration properties of nanoscale annular sector plates using non-local continuous medium theory. Pu<sup>[16]</sup> established the differential equations of motion and corresponding boundary conditions for in-plane free vibration of annular plates of functional gradient materials (FGM) in a thermal environment based on two-dimensional elasticity theory. Bagheri et al.<sup>[17-22]</sup> conducted an in-depth investigation of the mechanical behavior of annular plates in a thermal environment, including studies of the buckling behavior of annular plates under different external conditions<sup>[17-21]</sup> and a study of the thermally excited vibration behavior of FGM annular plates<sup>[22]</sup>, which greatly improved the theory of annular plate dynamics.

The spectral geometry method (SGM) is commonly used in dealing with the continuity of displacements of structures at boundaries, and it has received extensive attention and research in the academic field. Li<sup>[23]</sup> developed a general method based on the SGM for deriving sets of displacement functions that can be universally applied to various boundary conditions. Bao et al.<sup>[24]</sup> analyzed the transverse vibration characteristics of an arbitrary elastic boundary Euler-Bernoulli beam based on the non-local theory and SGM. Zhao<sup>[25]</sup> constructed the displacement functions of a rotating shell-like structure based on the principle of SGM. Zhang et al.<sup>[26]</sup> modeled the vibration behavior of a hyperboloid shell in a thermal environment based on SGM. Wang et al.<sup>[27-28]</sup> used SGM to establish the displacement function of Timoshenko beams with elastic constraints at the ends, and proposed a unified method to study Timoshenko beams with arbitrary variable cross-sections. In addition, the acoustic radiation properties of rectangular plates with submerged elastic boundary constraints were also investigated. Shi

et al.<sup>[29-30]</sup> analyzed the in-plane free vibration characteristics of annular plates under arbitrary boundary conditions, which improved the theory of static and dynamic characteristics of annular plates under arbitrary boundaries.

In summary, the research on the vibration characteristics of annular plates has been relatively complete, but there is still less research on the free vibration of annular plates in thermal environments, and there is also less comparative research on the vibration characteristics of open and closed annular plates. When using the boundary of a simulated spring-constrained plate, most of the research only considers a set of linear springs and a set of rotating springs in one direction, and there is still room for improvement in the calculation accuracy. In response to the above lack of research in the literature, this paper investigates the vibration characteristics of annular plates in a thermal environment by considering the changes in material properties caused by thermal strain and temperature increase within the annular plate surface. Three sets of linear springs and one set of rotating springs are used to simulate an arbitrary boundary of the annular plate, and circumferentially coupled springs are used to achieve continuity of the circumferential boundary of the closed annular plate. The theoretical model of the annular plate is constructed using the Rayleigh-Ritz method, and the vibration characteristics of the annular plate are solved. The vibration characteristics of the annular plate are solved and compared with the finite element results to verify the accuracy of the theoretical model.

## 1 Theoretical Analysis

Fig.1 shows the schematic diagram of the model of the annular plate. Four sets of springs are introduced to simulate arbitrary boundary conditions for the annular plate. When  $\varphi_0=360^\circ$ , coupling springs are introduced to ensure the continuity of the boundary displacements. In Fig.1(a),  $x$  and  $\theta$  are the radial and circumferential coordinates of the annular plate, respectively, and  $R$ ,  $r$ ,  $\varphi_0$ , and  $h$  denote the outer radius, inner radius, subtended angle and

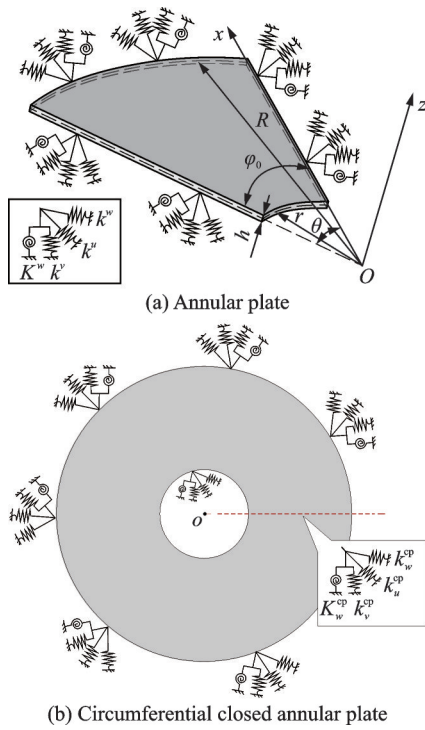


Fig.1 Schematic diagram of annular plate model

thickness of the annular plate, respectively. The annular plate is bounded by three sets of linear displacement restraint springs ( $k^u, k^v, k^w$ , in N/m) and one set of rotational restraint springs ( $K^w$ , in N·m/rad) along the  $x, \theta$ , and  $z$  coordinate directions to simulate the various complex boundary conditions of the plate. When  $\varphi_0=360^\circ$ , the two circumferential boundaries of the annular plate overlap and become a circular annular plate, as shown in Fig.1(b). Coupling springs are introduced at the coincident boundaries, including three sets of linear coupling springs ( $k_w^{cp}, k_u^{cp}, k_v^{cp}$ , in N/m) and one set of rotating coupling springs ( $K_w^{cp}$ , in N·m/rad) to ensure continuity of the boundaries.

As the annular plate in this paper is a plate structure with a small thickness, the effect of transverse shear can be ignored. Based on this, the theoretical model in this paper is derived based on the Kirchhoff's thin-plate theory. The strain in the annular plate can be expressed by the mid-plane displacement as

$$\begin{cases} \epsilon_x^0 = \frac{\partial u}{\partial x} \\ \epsilon_\theta^0 = \frac{1}{x} \frac{\partial v}{\partial \theta} + \frac{u}{x} \end{cases} \quad (1)$$

$$\epsilon_{x\theta}^0 = \frac{1}{x} \frac{\partial u}{\partial \theta} + \frac{\partial v}{\partial x} - \frac{v}{x} \quad (2)$$

$$\begin{cases} \kappa_x = -\frac{\partial^2 w}{\partial x^2} \\ \kappa_\theta = -\frac{1}{x^2} \frac{\partial^2 w}{\partial \theta^2} - \frac{1}{x} \frac{\partial w}{\partial x} \end{cases} \quad (3)$$

$$\tau_{x\theta} = -\frac{2}{x} \frac{\partial^2 w}{\partial \theta \partial x} + \frac{2}{x^2} \frac{\partial w}{\partial \theta} \quad (4)$$

where  $\epsilon_x, \epsilon_\theta$  and  $\epsilon_{x\theta}$  represent the positive strains along the  $x$  and  $\theta$  directions and the shear strain;  $\kappa_x, \kappa_\theta$  and  $\tau_{x\theta}$  the buckling strains; and  $u, v$  and  $w$  the displacements of the mid-plane face in the  $x, \theta$  and  $z$  directions, respectively. Considering the thermal effects arising from temperature changes, the thermal strain in the annular plate mid-plane can be expressed as

$$\epsilon_x^t = \alpha_x \Delta T, \epsilon_\theta^t = \alpha_\theta \Delta T, \epsilon_{x\theta}^t = \alpha_{x\theta} \Delta T \quad (5)$$

where  $\alpha_x, \alpha_\theta$  and  $\alpha_{x\theta}$  denote the coefficients of thermal expansion of the material in the  $x, \theta$  and tangential directions, respectively;  $\Delta T$  is the amount of temperature change in K. The total strain in the middle face of the annular plate is

$$\epsilon_x = \epsilon_x^0 - \epsilon_x^t, \epsilon_\theta = \epsilon_\theta^0 - \epsilon_\theta^t, \epsilon_{x\theta} = \epsilon_{x\theta}^0 - \epsilon_{x\theta}^t \quad (6)$$

As a result, the strain energy and the maximum kinetic energy kinetic of the annular plate structure can be expressed as

$$\begin{aligned} V_p = & \frac{K}{2} \int_0^{\varphi_0} \int_r^R \left( \epsilon_x^2 + \epsilon_\theta^2 + 2\mu\epsilon_x\epsilon_\theta + \frac{1-\mu}{2} \epsilon_{x\theta}^2 \right) x dx d\theta + \\ & \frac{D}{2} \int_0^{\varphi_0} \int_r^R \left( \kappa_x^2 + \kappa_\theta^2 + 2\mu\kappa_x\kappa_\theta + \frac{1-\mu}{2} \tau_{x\theta}^2 \right) x dx d\theta \end{aligned} \quad (7)$$

$$T_p = \frac{\rho h \omega^2}{2} \int_0^{\varphi_0} \int_r^R (w^2 + u^2 + v^2) x dx d\theta \quad (8)$$

where  $K= Eh/(1-\mu^2)$  and  $D= Eh^3/12(1-\mu^2)$  denote the tensile and flexural stiffness of the annular plate structure, respectively;  $E$  and  $\mu$  are the Young's modulus and the Poisson's ratio of the annular plate material, respectively. Assuming that the Young's modulus  $E$  decreases linearly with temperature, the expressions are

$$E = E_0 \times (1 - \beta \times \Delta T) \quad (9)$$

where  $E_0$  is the Young's modulus of the material at the initial temperature and  $\beta$  the sensitivity coefficient of Young's modulus relative to temperature.

The potential energy stored in the boundary-bound spring can be expressed as

$$\begin{aligned}
 V_b = & \frac{1}{2} \int_r^R [k_{\theta 0}^u u^2 + k_{\theta 0}^v v^2 + k_{\theta 0}^w w^2 + \\
 & K_{\theta 0}^w (\partial w / \partial \theta)^2 / x^2] \Big|_{\theta=0} dx + \\
 & \frac{1}{2} \int_r^R [k_{\theta 1}^u u^2 + k_{\theta 1}^v v^2 + k_{\theta 1}^w w^2 + \\
 & K_{\theta 1}^w (\partial w / \partial \theta)^2 / x^2] \Big|_{\theta=\varphi_0} dx + \\
 & \frac{1}{2} \int_0^{\varphi_0} [k_{x0}^u u^2 + k_{x0}^v v^2 + k_{x0}^w w^2 + \\
 & K_{x0}^w (\partial w / \partial x)^2] \Big|_{x=0} (R-r) d\theta + \\
 & \frac{1}{2} \int_0^{\varphi_0} [k_{x1}^u u^2 + k_{x1}^v v^2 + k_{x1}^w w^2 + \\
 & K_{x1}^w (\partial w / \partial x)^2] \Big|_{x=R} (R-r) d\theta \quad (10)
 \end{aligned}$$

In summary, the Lagrangian function  $L_p$  of the annular plate structure can be expressed as

$$L_p = V_p + V_b - T_p \quad (11)$$

When  $\varphi_0 = 360^\circ$ , the potential energy stored in the coupled constrained spring can be expressed as

$$\begin{aligned}
 V_{cp} = & \frac{1}{2} \left\{ k_w^{cp} (w|_{\theta=0} - w|_{\theta=2\pi})^2 + \right. \\
 & k_u^{cp} (u|_{\theta=0} - u|_{\theta=2\pi})^2 + k_v^{cp} (v|_{\theta=0} - v|_{\theta=2\pi})^2 + \\
 & \left. K_w^{cp} \left( \frac{1}{x} \frac{\partial w}{\partial \theta} \Big|_{\theta=0} - \frac{1}{x} \frac{\partial w}{\partial \theta} \Big|_{\theta=2\pi} \right)^2 dx \right\} \quad (12)
 \end{aligned}$$

In this paper, a modified Fourier series is used and auxiliary functions are introduced to ensure the continuity of the displacement function and its derivatives at the boundary. The displacement function of the annular plate can be expressed as<sup>[24]</sup>

$$u(x, \theta) = \sum_{m=-2}^{\infty} \sum_{n=-2}^{\infty} A_{m,n}^u \Theta_m \Theta_n \quad (13)$$

$$v(x, \theta) = \sum_{m=-2}^{\infty} \sum_{n=-2}^{\infty} A_{m,n}^v \Theta_m \Theta_n \quad (14)$$

$$w(x, \theta) = \sum_{m=-4}^{\infty} \sum_{n=-4}^{\infty} A_{m,n}^w \Theta_m \Theta_n \quad (15)$$

where  $A_{m,n}^u$ ,  $A_{m,n}^v$  and  $A_{m,n}^w$  represent the unknown Fourier coefficient matrixes of displacements; and  $\Theta_m$  and  $\Theta_n$  the trigonometric functions corresponding to  $m$  and  $n$ , expressed as

$$\Theta_m = \begin{cases} \sin(\lambda_m x) & m < 0 \\ \cos(\lambda_m x) & m \geq 0 \end{cases}, \Theta_n = \begin{cases} \sin(\lambda_n \theta) & n < 0 \\ \cos(\lambda_n \theta) & n \geq 0 \end{cases} \quad (16)$$

where  $\lambda_m = m\pi/L$ ,  $\lambda_n = n\pi/\varphi_0$ . When  $m < 0$  or  $n < 0$ ,  $\Theta_m$  and  $\Theta_n$  are the auxiliary functions whose purpose is to eliminate the discontinuity of the boundary displacements.

The Rayleigh-Ritz method is used to conduct variational operations on the Lagrange function of plate structure, shown as

$$\frac{\partial L}{\partial \vartheta} = 0 \quad \vartheta = A_{m,n}^u, A_{m,n}^v, A_{m,n}^w \quad (17)$$

Truncation of the levels at  $m=M$  and  $n=N$  gives a free vibrational equation of dimension  $(M+5) \times (N+5) + 2 \times (M+3) \times (N+3)$ , expressed as

$$(K - \omega^2 M) A = 0 \quad (18)$$

where  $K$ ,  $M$  and  $A$  represent the stiffness matrix, mass matrix, and Fourier displacement coefficient matrix of the annular plate respectively.

## 2 Results and Discussion

### 2.1 Setting of boundary conditions

In this paper, four sets of boundary springs are used to achieve constraints on the boundary conditions of the annular plate, and arbitrary boundary conditions can be achieved by changing the stiffness values. In this paper, C, S, and F are used to represent the clamped, simply supported, and free boundaries, and  $E_1$ ,  $E_2$  and  $E_3$  are the three elastic boundaries with spring stiffness coefficients<sup>[9]</sup>. Each boundary condition is shown in Table 1.

**Table 1 Each boundary condition corresponding to the spring stiffness value**

Type of boundary	Spring stiffness value			
	$k_u/D$	$k_v/D$	$k_w/D$	$K_w/D$
F	0	0	0	0
C	$10^{15}$	$10^{15}$	$10^{15}$	$10^{15}$
S	$10^{15}$	$10^{15}$	$10^{15}$	0
$E_1$	$10^{15}$	$10^{15}$	$10^4$	$10^{15}$
$E_2$	$10^4$	$10^{15}$	$10^{15}$	$10^{15}$
$E_3$	$10^{15}$	$10^4$	$10^{15}$	$10^{15}$

### 2.2 Convergence and accuracy verification

This section verifies the convergence and accuracy of the theoretical approach used in the previous section. The results of this paper are first compared

with those in the literature. To facilitate the comparison, the dimensionless frequency parameter  $\lambda^2 = \omega a^2 (\rho h / D)^{1/2}$  is introduced and set to  $r/R = 0.1$ . Table 2 shows the comparison of the dimensionless frequency parameters of the annular plate under different boundary conditions and different cut-off coefficients with the calculated results obtained by using the DQM in Ref. [10], the annular plate used is a circumferentially closed circular plate with a radius ratio  $r/R = 0.1$ . The results in the table show that after  $M=N=10$ , the results of this paper agree very well with those in Ref. [10], which verifies the convergence and accuracy of the method used in this paper.

The next step is to verify the accuracy of the theoretical model in this paper under different temperature environments. Tables 3 and 4 show the first eight order natural frequencies of the annular plate ( $\varphi_0 = 45^\circ$ ) and the circular annular plate ( $\varphi_0 = 360^\circ$ ) calculated by the present method and FEM for different boundary conditions at  $\Delta T = 0, 20$ , and 60 K, respectively. Set the annular plate dimensions:  $R = 1$  m,  $r = 0.3$  m,  $h = 0.01$  m, material parameters:  $E = 200$  GPa,  $\mu = 0.3$ ,  $\rho = 7850$  kg/m<sup>3</sup>,

**Table 2 Comparison of the frequency parameter**

Boundary condition	Present, $M=N$				DQM <sup>[10]</sup>
	2	6	10	14	
C-C	28.36	27.30	27.28	27.28	27.28
C-S	19.73	17.80	17.79	17.79	17.79
C-F	4.29	4.24	4.24	4.24	4.24
S-C	23.29	22.70	22.70	22.70	22.70
S-S	14.55	14.49	14.49	14.49	14.49
S-F	3.96	3.96	3.45	3.45	3.45
F-C	10.32	10.16	10.16	10.16	10.16
F-S	5.40	4.86	4.85	4.85	4.85
F-F	9.84	8.78	8.78	8.78	8.78

$\alpha = 1.2 \times 10^{-5}$ ,  $\beta = 5 \times 10^{-3}$ . FEM uses the ANSYS software for modeling calculations, using SHELL181 cells. As can be seen from Tables 3 and 4, when  $M=N=14$ , the modal numerical solution obtained by this method is basically in good agreement with the finite element calculation results. The slight numerical differences may be because FEM uses a different plate theory for the solution and the accuracy of the calculation results is related to the degree of mesh refinement. This is a good indication that the convergence and accuracy of the present method are reliable.

**Table 3 The first eight order natural frequencies of the annular plate ( $\varphi_0 = 45^\circ$ ) obtained by two methods**

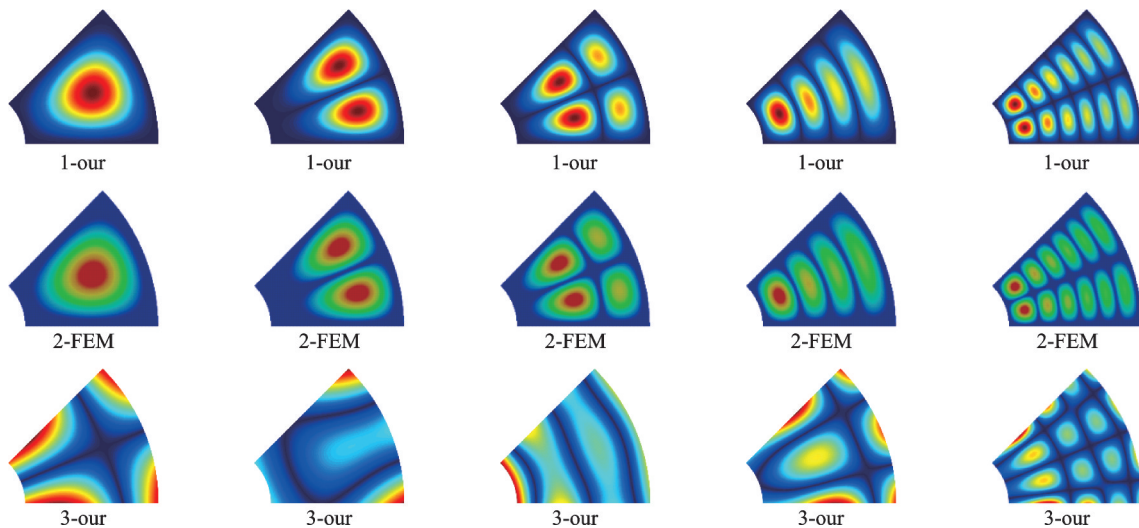
Mode order			1	2	3	4	5	6	7	8	Hz
$\Delta T = 0$	C-C-C-C	$M=N=14$	262.81	474.36	545.21	763.14	856.27	918.47	1147.03	1208.48	
		FEM	262.34	472.44	542.80	758.05	849.94	911.41	1135.80	1195.80	
	S-S-S-S	$M=N=14$	139.90	313.26	361.57	566.94	623.96	676.10	912.90	932.56	
		FEM	139.75	312.55	360.63	564.61	621.17	672.82	906.91	926.34	
	F-F-F-F	$M=N=14$	106.48	109.57	138.75	248.23	310.47	326.44	341.01	471.78	
		FEM	105.93	109.25	138.35	246.32	309.50	324.56	338.81	467.32	
$\Delta T = 20$	C-C-C-C	$M=N=14$	249.32	450.02	517.23	723.98	812.33	871.34	1088.17	1146.46	
		FEM	248.88	448.20	514.95	719.15	806.32	864.64	1077.51	1134.44	
	S-S-S-S	$M=N=14$	132.72	297.18	343.02	537.85	591.94	641.40	866.05	884.70	
		FEM	132.58	296.51	342.12	535.64	589.29	638.29	860.37	878.80	
	F-F-F-F	$M=N=14$	101.02	103.95	131.63	235.49	294.54	309.69	323.51	447.57	
		FEM	100.49	103.64	131.25	233.68	293.62	307.90	321.42	443.34	
$\Delta T = 60$	C-C-C-C	$M=N=14$	219.88	396.88	456.16	638.49	716.41	768.45	959.67	1011.09	
		FEM	219.49	395.27	454.14	634.23	711.11	762.54	950.28	1000.48	
	S-S-S-S	$M=N=14$	117.05	262.09	302.51	474.34	522.04	565.67	763.79	780.24	
		FEM	116.92	261.50	301.72	472.39	519.71	562.92	758.78	775.03	
	F-F-F-F	$M=N=14$	89.09	91.67	116.09	207.68	259.76	273.12	285.31	394.72	
		FEM	88.63	91.41	115.75	206.09	258.95	271.55	283.47	390.99	

**Table 4 The first eight order natural frequencies of ring plate ( $\varphi_0=360^\circ$ ) obtained by two methods**

			Hz							
Mode order			1	2	3	4	5	6	7	8
$\Delta T=0$	C-C	$M=N=14$	110.24	113.39	113.40	124.32	124.32	145.94	145.94	179.76
		FEM	110.23	113.37	113.37	124.26	124.26	145.82	145.82	179.54
	S-S	$M=N=14$	51.24	56.68	56.68	73.60	73.60	101.88	101.88	139.90
		FEM	51.23	56.66	56.66	73.56	73.56	101.81	101.81	139.75
	F-F	$M=N=14$	11.93	11.93	20.31	29.82	29.82	44.47	44.47	52.95
		FEM	11.91	11.91	20.31	29.78	29.78	44.28	44.28	52.87
$\Delta T=20$	C-C	$M=N=14$	104.58	107.57	107.58	117.94	117.94	138.45	138.45	170.54
		FEM	104.57	107.55	107.55	117.88	117.88	138.34	138.34	170.33
	S-S	$M=N=14$	48.61	53.77	53.77	69.82	69.82	96.65	96.65	132.72
		FEM	48.60	53.75	53.75	69.79	69.79	96.59	96.59	132.58
	F-F	$M=N=14$	11.32	11.32	19.27	28.29	28.29	42.19	42.19	50.23
		FEM	11.30	11.30	19.27	28.25	28.25	42.01	42.01	50.16
$\Delta T=60$	C-C	$M=N=14$	92.23	94.87	94.88	104.01	104.01	122.10	122.10	150.40
		FEM	92.23	94.85	94.85	103.96	103.96	122.00	122.00	150.21
	S-S	$M=N=14$	42.87	47.42	47.42	61.58	61.58	85.24	85.24	117.05
		FEM	42.86	47.41	47.41	61.54	61.54	85.18	85.18	116.92
	F-F	$M=N=14$	9.98	9.98	16.99	24.95	24.95	37.21	37.21	44.30
		FEM	9.96	9.96	16.99	24.92	24.92	37.05	37.05	44.23

Among the three boundary conditions, the annular plate has the highest natural frequencies at the C-C-C-C boundary and the lowest at the F-F-F-F boundary. This is because the increase in the boundary constraint makes the plate structure stiffer and thus increases the natural frequencies of the plate. As the temperature increases, the plate structure suffers from thermal stresses and softening of Young's modulus and its natural frequencies de-

crease. The 1st, 3rd, 5th, 7th, and 22nd order modal shapes of the annular plate ( $\varphi_0=45^\circ$ ) obtained by this method and the FEM at the C-C-C-C, S-S-S-S, F-F-F-F boundaries and the circular annular plate ( $\varphi_0=360^\circ$ ) at the C-C, S-S, F-F boundary conditions at  $\Delta T=60$  K are given in Figs.2, 3. It can be seen that the modal shapes obtained by the two methods are in good agreement, which verifies the accuracy of the method.



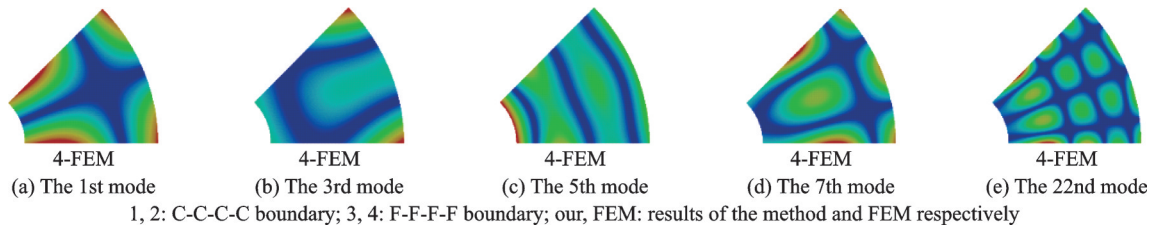


Fig.2 Comparison of vibration modes of annular plates ( $\varphi_0=45^\circ$ ) obtained by the method and FEM

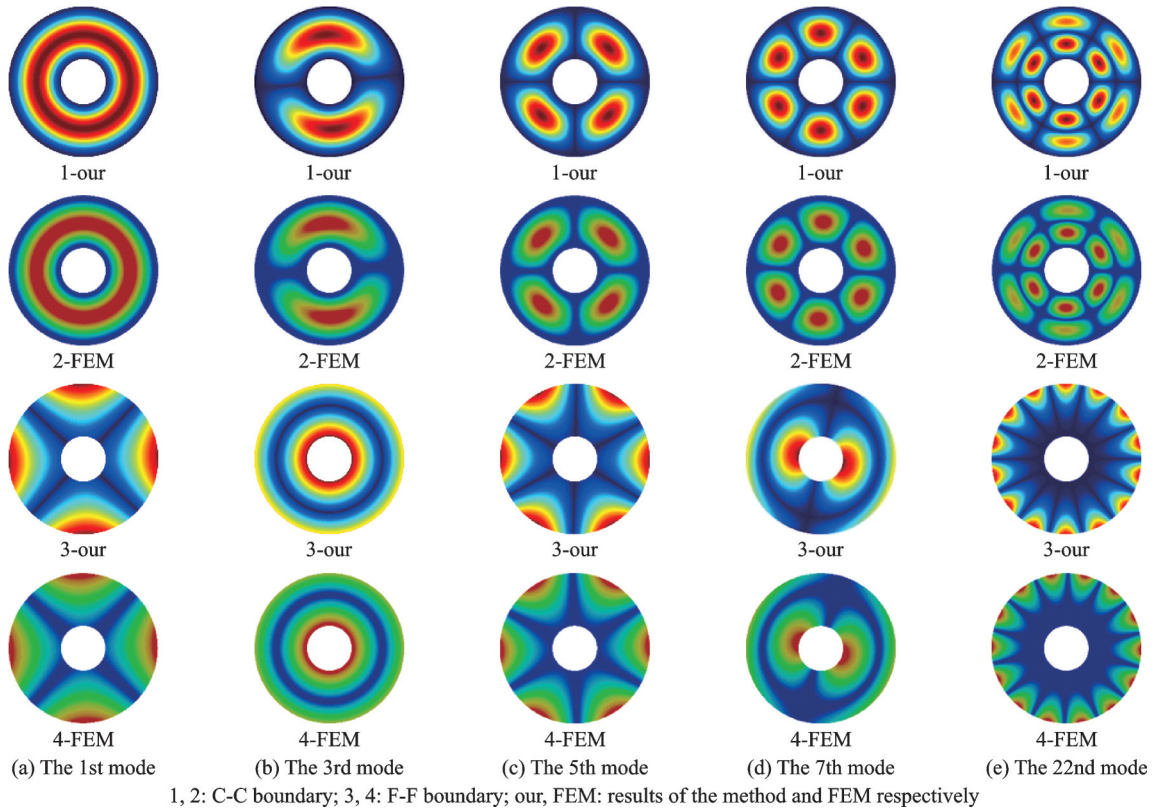


Fig.3 Comparison of vibration modes of annular plates ( $\varphi_0=360^\circ$ ) obtained by the method and FEM

### 2.3 Parametric analysis

The accuracy of the theoretical model used in this paper has been verified in the previous section, and the next step is to carry out a parametric analysis of the annular plate structure. Firstly, the effect of the magnitude of the subtended angle  $\varphi_0$  on the natural frequencies of the annular plate structure in the thermal environment is investigated. The dimensions of the annular plate used for the calculations in the previous section are used, and the two planar boundaries of the open annular plate are set as free boundaries, while the remaining two curved boundaries are classical or elastic. Fig.4 gives the fractal scatter diagram for different  $\varphi_0$  corresponding to the natural frequencies of the annular plate at  $\Delta T=100$  K for the S-S, C-C, F-F,  $E_1-E_2$ ,  $E_2-E_3$ , and  $E_1-E_3$  boundary conditions, with  $\varphi_0$  taking values

from  $15^\circ$  to  $360^\circ$ . It can be seen from Fig.4 that when  $\varphi_0 < 360^\circ$ , the 1st order natural frequency of the annular plate under the remaining boundaries, except for the F-F boundary, increases with the increase of the  $\varphi_0$ ; the 2nd, 3rd, and 4th order natural frequencies under the S-S, C-C, F-F, and  $E_1-E_2$  boundaries decrease with the increase of the  $\varphi_0$ ; under both the  $E_2-E_3$  and  $E_1-E_3$  elastic boundaries, the 2nd, 3rd and 4th natural frequencies of the plate decrease overall as the  $\varphi_0$  becomes larger, but fluctuate at some angles. At  $\varphi_0=360^\circ$ , the first four order natural frequencies at all six boundaries increase slightly due to the addition of coupling springs at the two planar boundaries of the annular plate increasing the stiffness of the structure. Among these six boundary conditions, the first four natural frequencies of the annular plate structure are the highest un-

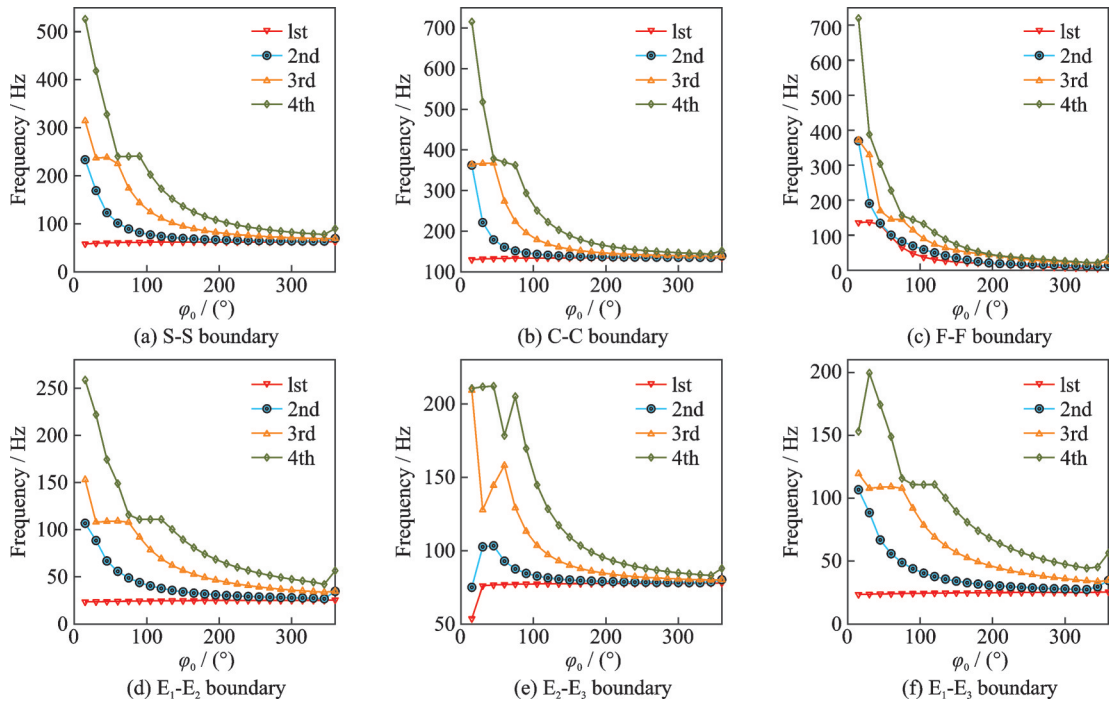


Fig.4 Influence of subtended angle  $\varphi_0$  on natural frequency of the annular plate under different boundary conditions at  $\Delta T=100$  K

der the C-C boundary condition. This is because the plate has the most boundary-bound springs under the C-C boundary condition, which makes the overall stiffness of the plate greater than that under other boundaries. An interesting phenomenon is that the plate structure also has high natural frequencies at the F-F boundary when  $\varphi_0$  is small. This is because we have neglected the first six natural frequencies with zero values at the free boundary, which correspond to the six rigid body motion modes of the plate structure. In addition to this, the fundamental frequency of the plate structure under the  $E_2$ - $E_3$  boundary is significantly higher than those under  $E_1$ - $E_2$  and  $E_1$ - $E_3$  for the three elastic boundary conditions.

Next, the effect of the ratio  $r/R$  of the annular plate on the natural frequency of the structure in a thermal environment is analyzed, using the thickness of the annular plate used for the calculations in the previous section. Figs. 5 and 6 show the influence of the ratio  $r/R$  on the natural frequencies of two types of annular plate,  $\varphi_0=45^\circ$  and  $\varphi_0=360^\circ$ , at  $\Delta T=100$  K for classical and elastic boundary conditions respectively.  $r/R$  is taken to be from 0.1 to

0.8 and the first 10 order natural frequencies are observed.

For all three classical boundary conditions, the natural frequencies of the annular plate increase with increasing  $r/R$  when  $\varphi_0=45^\circ$ . This is because when  $R$  is constant, the increase in  $r/R$  reduces the mass of the annular plate, while the reduction in stiffness is not significant in comparison. Therefore, the overall inherent frequency is in an increasing trend. However, it is worth noting that at the F-F-F-F boundary, this trend is not obvious for the fundamental frequencies. As the mode order increases, the natural frequencies tend to increase with increasing  $r/R$ , and the natural frequencies of the annular plate tend to increase with increasing mode order for all three boundary conditions.

When  $\varphi_0=360^\circ$ , with the increase of  $r/R$ , the natural frequencies of the circular annular plate under the F-F boundary change gently, and its natural frequencies gradually decrease in the first four orders, and from the 5th order onwards, the results no longer varies monotonically, and a small fluctuation appears, which is very different from the results under the two outer boundaries, and under the C-C

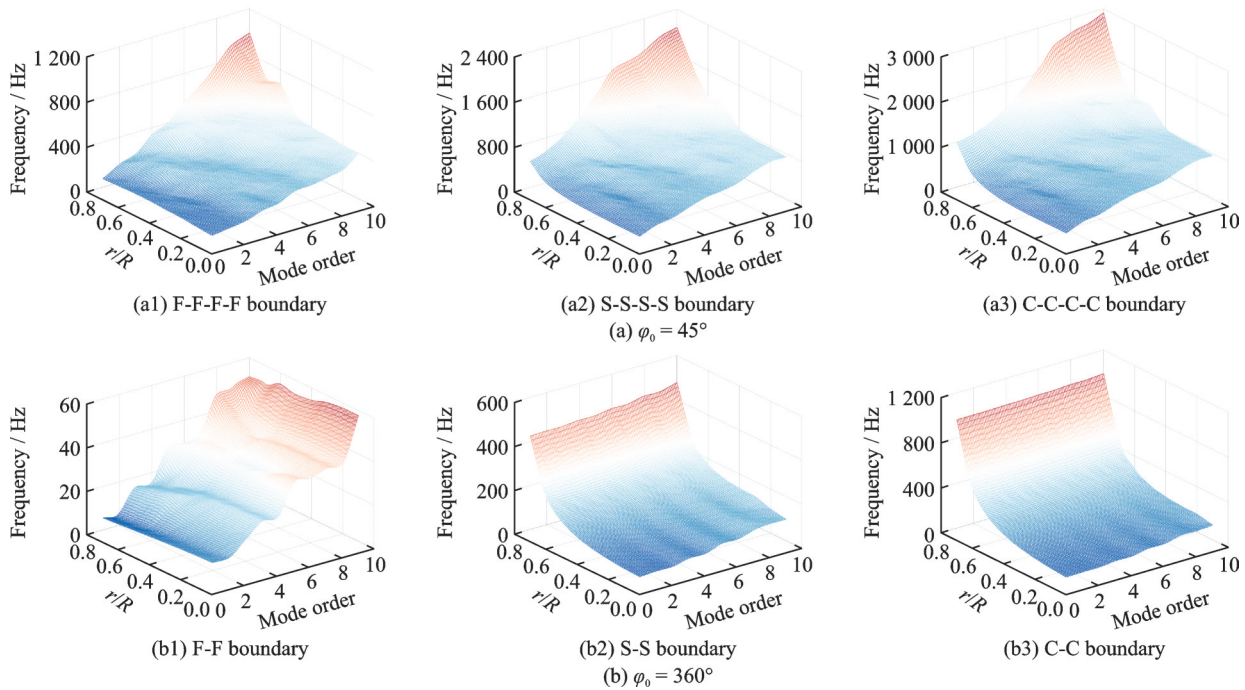


Fig.5 Influence of  $r/R$  on the natural frequency of the annular plate under classical boundary conditions at  $\Delta T=100$  K

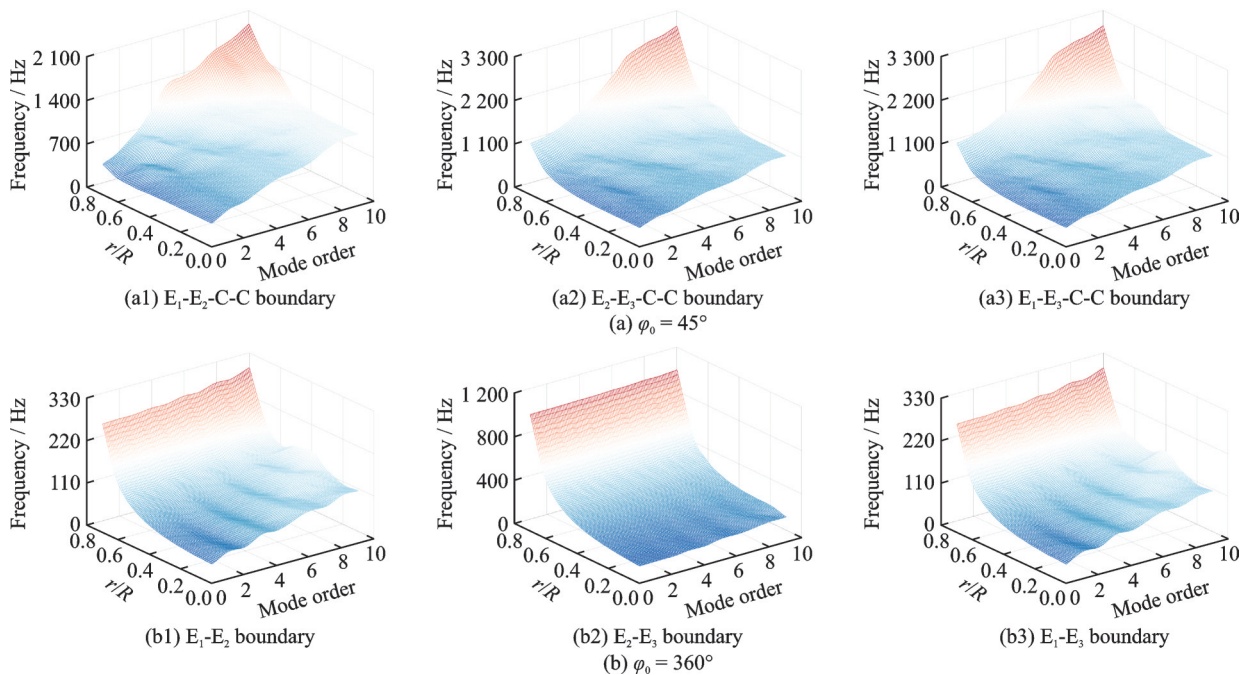


Fig.6 Influence of  $r/R$  on the natural frequency of the annular plate under elastic boundary conditions at  $\Delta T=100$  K

boundary and S-S boundary, the natural frequencies of the circular annular plate increase with the increase of  $r/R$ , and the larger the value of  $r/R$  is, the more obvious this trend is. With the increase of the mode order, the natural frequencies of the circular annular plate have a great tendency to rise under the F-F boundary, while the change is more gentle under the C-C and S-S boundaries. When the bound-

ary conditions are elastic boundaries, i.e. as shown in Fig.6, it can be seen that the plate has the highest natural frequencies under the  $E_2-E_3$  boundary and the trend of change is similar to that under the C-C boundary; the change in natural frequencies under the  $E_1-E_2$  and  $E_1-E_3$  boundaries is very similar for  $\varphi_0=360^\circ$ , which is because the direction of the small stiffness spring restraint in both  $E_2$  and  $E_3$

boundaries is parallel to the midplane of the circular annular plate, so the effect of the restraint is close. The natural frequencies of the annular plate are significantly higher for the  $E_2$ - $E_3$  boundary conditions than the results for the other two elastic boundary conditions, especially when  $r/R$  takes on larger values, indicating that the constraint in the  $z$ -axis direction has the greatest effect on the vibration of the annular plate.

### 3 Conclusions

The vibration characteristics of the annular plate in a thermal environment are investigated by considering the changes in Young's modulus of the material caused by thermal strain and temperature increase within the annular plate face. The boundary of the annular plate is constrained by virtual springs and the coupling of the overlapping boundary of the circular annular plate is realized. The theoretical model of the annular plate is constructed using the Rayleigh-Ritz method and the accuracy of the theoretical model in this paper is verified by comparing it with the finite element results. Based on the correctness, a parametric analysis of the annular plate structure was carried out. The following conclusions were obtained:

(1) As the temperature increases, the annular plate is subjected to thermal stress and softening of Young's modulus, and the natural frequencies of the annular plate gradually decrease.

(2) When  $\varphi_0 < 360^\circ$ , the 1st order natural frequency of the annular plate increases with the increase of  $\varphi_0$ , and the 2nd, 3rd, and 4th order natural frequencies decrease with the increase of  $\varphi_0$ . Under the two elastic boundaries of  $E_2$ - $E_3$  and  $E_1$ - $E_3$ , the 2nd, 3rd and 4th natural frequencies as a whole decrease with the increase of  $\varphi_0$ , but in some angles there are fluctuations. When  $\varphi_0 = 360^\circ$ , there is a slight increase in the first four orders of natural frequencies.

(3) When  $\varphi_0 = 45^\circ$ , the natural frequencies of the annular plate increase with increasing  $r/R$  under classical boundaries. As the mode order increases,

the tendency of the natural frequencies increasing with increasing  $r/R$  becomes more and more obvious. When  $\varphi_0 = 360^\circ$ , with the increase of  $r/R$ , the natural frequencies of the circular annular plate under the F-F boundary change gently; under the C-C boundary and S-S boundary, the results increase with the increase of  $r/R$ . When the boundary condition is the elastic boundary, the plate has the natural frequencies under  $E_2$ - $E_3$  boundary.

### References

- [1] ZHOU Weiya, WU Shunan, WANG Enmei. Distributed vibration control of satellite solar panels based on consensus theory[J]. Journal of Nanjing University of Aeronautics & Astronautics, 2021, 53(6): 909-917. (in Chinese)
- [2] IRIE T, YAMADA G, MURAMOTO Y. Natural frequencies of in-plane vibration of annular plates[J]. Journal of Sound and Vibration, 1984, 97(1): 171-175.
- [3] CIVALEK O, DASTJERDI S, et al. Buckling and free vibrations of CNT-reinforced cross-ply laminated composite plates[J]. Mechanics Based Design of Structures and Machines, 2022, 50(6): 1914-1931.
- [4] CIVALEK O, AVCAR M. Free vibration and buckling analyses of CNT reinforced laminated non-rectangular plates by discrete singular convolution method[J]. Engineering with Computers, 2022, 38(4): 489-521.
- [5] MERCAN K, BALTACIOGLU A K, CIVALEK Ö. Free vibration of laminated and FGM/CNT composites annular thick plates with shear deformation by discrete singular convolution method[J]. Composite Structures, 2018, 186: 139-153.
- [6] ERSOY H, MERCAN K, CIVALEK Ö. Frequencies of FGM shells and annular plates by the methods of discrete singular convolution and differential quadrature methods[J]. Composite Structures, 2018, 183: 7-20.
- [7] DASTJERDI S, AKGOZ B, CIVALEK Ö, et al. On the non-linear dynamics of torus-shaped and cylindrical shell structures[J]. International Journal of Engineering Science, 2020, 156: 103371.
- [8] DASTJERDI S, AKGOZ B, CIVALEK Ö, et al. On the effect of viscoelasticity on behavior of gyroscopes[J]. International Journal of Engineering Science, 2020, 149: 103236.
- [9] SOBHANI E, MASOODI A, CIVALEK Ö, et al.

- Agglomerated impact of CNT vs. GNP nanofillers on hybridization of polymer matrix for vibration of coupled hemispherical-conical-conical shells[J]. *Aerospace Science and Technology*, 2021, 120: 107257.
- [10] SOBHANI E, ARBABIAN A, CIVALEK Ö, et al. The free vibration analysis of hybrid porous nanocomposite joined hemispherical-cylindrical-conical shells[J]. *Engineering with Computers*, 2022, 38(4): 3125-3152.
- [11] HAN J B, LIEW K M. Axisymmetric free vibration of thick annular plates[J]. *International Journal of Mechanical Sciences*, 1999, 41(9): 1089-1109.
- [12] TORNABENE F, VIOLA E, INMAN D J. 2-D differential quadrature solution for vibration analysis of functionally graded conical, cylindrical shell and annular plate structures[J]. *Journal of Sound and Vibration*, 2009, 328(3): 259-290.
- [13] EFRAIM E, EISENBERGER M. Exact vibration analysis of variable thickness thick annular isotropic and FGM plates[J]. *Journal of Sound and Vibration*, 2007, 299(4/5): 720-738.
- [14] KE L L, YANG J, KITIPORNCHAI S, et al. Bending, buckling and vibration of size-dependent functionally graded annular microplates[J]. *Composite Structures*, 2012, 94(11): 3250-3257.
- [15] GÜRSES M, AKGÖZ B, CIVALEK Ö, et al. Mathematical modeling of vibration problem of nano-sized annular sector plates using the nonlocal continuum theory via eight-node discrete singular convolution transformation[J]. *Applied Mathematics and Computation*, 2012, 219(6): 3226-3240.
- [16] PU Yu. In-plane free vibration analysis of functionally graded annular plates under thermal environment[D]. Lanzhou: Lanzhou University of Technology, 2013. (in Chinese)
- [17] BAGHERI H, KIANI Y, ESLAMI M R, et al. Asymmetric thermal buckling of annular plates on a partial elastic foundation[J]. *Journal of Thermal Stresses*, 2017, 40(8): 1015-1029.
- [18] BAGHERI H, KIANI Y, ESLAMI M R, et al. Asymmetric thermo-inertial buckling of annular plates[J]. *Acta Mechanica*, 2017, 228(4): 1493-1509.
- [19] BAGHERI H, KIANI Y, ESLAMI M R, et al. Asymmetric thermal buckling of temperature dependent annular FGM plates on a partial elastic foundation[J]. *Computers and Mathematics with Applications*, 2018, 75(5): 1566-1581.
- [20] BAGHERI H, KIANI Y, ESLAMI M R, et al. Asymmetric compressive stability of rotating annular plates[J]. *European Journal of Computational Mechanics*, 2019, 28(4): 325-350.
- [21] BAGHERI H, KIANI Y, ESLAMI M R, et al. Buckling of moderately thick annular plates subjected to torque[J]. *Archive of Mechanical Engineering*, 2019, 66(2): 209-227.
- [22] BAGHERI H, KIANI Y, ESLAMI M R, et al. Rapid heating vibrations of FGM annular sector plates[J]. *Engineering with Computers*, 2021, 37(1): 305-322.
- [23] LI W L. Vibration analysis of rectangular plates with general elastic boundary supports[J]. *Journal of Sound and Vibration*, 2004, 273(3): 619-635.
- [24] BAO Siyuan, CAO Jinrui, ZHOU Jing. Transverse vibration characteristics of nonlocal beams with arbitrary elastic boundary conditions[J]. *Journal of Vibration Engineering*, 2020, 33(2): 276-284. (in Chinese)
- [25] ZHAO Yunke. Research of vibration characteristics for shells of revolution and coupled structures subjected to arbitrary boundary conditions[D]. Harbin: Harbin Engineering University, 2017. (in Chinese)
- [26] ZHANG Y F, ZHU Z Y, WANG G. Thermal modal analysis of doubly curved shell based on Rayleigh-Ritz method[J]. *Transactions of Nanjing University of Aeronautics and Astronautics*, 2022, 39(1): 58-65.
- [27] WANG G, LI W L, LIU T S. The average radiation efficiency of a plate immersed in water with general boundary conditions[J]. *Mechanics Research Communications*. 2020, 106: 103532.
- [28] WANG G, LI W L, LI W Y, et al. A unified procedure for the vibration analysis of elastically restrained Timoshenko beams with variable cross sections[J]. *Noise Control Engineering Journal*, 2020, 68(1): 38-47.
- [29] SHI Xianjie. The construction and analysis on unified dynamical model of revolve structures subjected to complex boundary conditions[D]. Harbin: Harbin Engineering University, 2014. (in Chinese)
- [30] SHI Dongyan, SHI Xianjie, LI Wenlong. In-plane vibration analysis of annular sector plates with arbitrary boundary supports[J]. *Journal of Vibration Engineering*, 2014, 27(1): 1-8. (in Chinese)

**Acknowledgements** This work was supported by the National Natural Science Foundation of China (No.51805341), the Natural Science Foundation of Jiangsu Province (Nos. BK20220500, BK20180843), the Jiangsu Funding Program for Excellent Postdoctoral Talent (No. 20220ZB560), and the Postgraduate Research & Practice Innovation Program of

Jiangsu Province.

**Authors** Mr. ZHU Ziyuan received the B.S. degree from School of Mechanical and Electrical Engineering, Soochow University in 2021, and is currently pursuing the M.A.Eng in School of Mechanical and Electrical Engineering, Soochow University. His research interests include vibration and noise control.

Prof. WANG Gang received the B.S. and Ph.D. degrees from Harbin Engineering University, Harbin, China, in 2010 and 2016, respectively. From 2013 to 2015, he was pursuing a co-training Ph.D. at Wayne State University. His research interests include dynamics analysis, vibration and

noise control, etc.

**Author contributions** Mr. ZHU Ziyuan completed the calculation of data results and simulation comparison, and wrote the third and fourth parts of the manuscript. Mr. XU Ruikang integrated the theoretical model and completed the first and second parts of the manuscript. Prof. WANG Gang designed the study, compiled the models, and reviewed the manuscript. All authors commented on the manuscript draft and approved the submission.

**Competing interests** The authors declare no competing interests.

(Production Editor: ZHANG Huangqun)

## 热环境下复杂边界环形板振动特性建模及分析

朱梓渊, 徐瑞康, 王 刚

(苏州大学机电工程学院, 苏州 215131, 中国)

**摘要:**提出一种统一的方法来预测环形板在稳态热环境下的自由振动行为。基于谱几何法(Spectral geometry method, SGM),采用改进的傅里叶级数展开环形板的位移。基于一阶剪切变形理论(First-order shear deformation theory, FSDT)得到了环形板的势能和最大动能。采用三组线性弹簧和一组旋转弹簧模拟环形板的任意边界,使用周向耦合弹簧以保证回转角为 $360^\circ$ 的圆环板周向边界的连续性,结合瑞利-里兹法构建环形板的理论模型,求解环形板的振动特性,通过与有限元(Finite element method, FEM)计算结果的对比,验证了该方法的准确性。本文采用无网格法,与目前主流的方法(如有限元法)相比,其计算效率更高。本文还研究了环形板的模态数值解和边界条件、内外半径比之间的关系。本文为环形板在工程实践中的应用提供了参考。

**关键词:**环形板;谱几何法;热环境;瑞利-里兹法